

Article

# Degradation Products on Byzantine Glasses from Northern Tunisia

Valeria Comite <sup>1</sup>, Martina Andreoli <sup>2</sup>, Davide Atzei <sup>3</sup>, Donatella Barca <sup>4</sup>,  
Marzia Fantauzzi <sup>3</sup>, Mauro Francesco La Russa <sup>4</sup>, Antonella Rossi <sup>3</sup>, Vittoria Guglielmi <sup>1</sup>  
and Paola Fermo <sup>1,\*</sup>

<sup>1</sup> Dipartimento di Chimica, Università degli Studi di Milano, 20133 Milano, Italy; valeria.comite@unimi.it (V.C.); vittoria.guglielmi@unimi.it (V.G.)

<sup>2</sup> Dipartimento di Lettere e Filosofia, Università degli Studi di Trento, 38100 Trento, Italy; martina.andreoli@unitn.it

<sup>3</sup> Dipartimento di Scienze Chimiche e Geologiche, Università degli Studi di Cagliari, 09042 Monserrato, Italy; datzei@unica.it (D.A.); fantauzzi@unica.it (M.F.); rossi@unica.it (A.R.)

<sup>4</sup> Dipartimento di Biologia, Ecologia e Scienze della Terra (DiBEST), Università della Calabria, 87036 Rende, Italy; donatella.barca@unical.it (D.B.); mauro.larussa@unical.it (M.F.L.R.)

\* Correspondence: paola.fermo@unimi.it

Received: 22 September 2020; Accepted: 23 October 2020; Published: 26 October 2020



**Abstract:** This study deals with the identification of the degradation products present on some Byzantine glasses coming from an archaeological excavation in Northern Tunisia. The main purpose of the present investigation is the identification of the products and the characterization of surface altered points, namely iridescent and black patinas, which are present on some selected glasses. Non-destructive techniques such as XPS (X-ray Photoelectron Spectroscopy), SEM-EDS (Scanning Electron Microscopy coupled with Energy Dispersive Spectroscopy), ATR-FTIR (Attenuated Total Reflection-Fourier Infrared Spectroscopy) and LA-ICP-MS (Laser-Ablation Inductively Coupled Plasma-Mass Spectrometry) are here exploited. SEM-EDS was employed to ascertain the morphological structure and the chemical composition of various points, apparently different, on the glass surfaces. Small area XPS was performed for identifying the elements present on the sample surface, for determining their chemical state and for establishing the atomic composition of the morphologically different regions. LA-ICP-MS was exploited to determine the chemical composition as far as the trace elements are concerned. The presence of iridescent patinas and of encrustations has been highlighted on the glass surfaces in correspondence to the altered areas: iridescent patinas are due to the fact that the glasses are depleted in alkali and alkaline earths. The encrustations resulted due to the presence of calcium carbonates, and/or oxyhydroxides. In one case sulfides were also detected by SEM.

**Keywords:** Byzantine glass; degradation products; patinas; XPS; LA/ICP-MS; SEM-EDS; FTIR

## 1. Introduction

A very interesting aspect concerning archaeological glass analysis is represented by the study of the degradation and corrosion processes [1–7]. Surface alteration is due to burial conditions and depends on different parameters such as temperature, humidity, pH [8] glass-composition and pollution. In particular, both soil and groundwater compositions, if the objects were buried, play an important role in the glass degradation phenomena. Other factors include the exposure time, the temperature (especially fluctuating temperatures), the amount of water that comes in contact with the surface and the alkalinity or acidity of the burial environment [8,9]. It has also been demonstrated that

archaeological glass objects found in dry soils are better preserved than those found in moist soils, as water is acknowledged to be one of the main causes of glass weathering [9].

Furthermore, the stability of an ancient glass is even worse due to the presence of elements such as alkali and alkaline earths, which have weaker bonds to oxygen within the glass network [10,11].

Among the glass constituents, sodium carbonate decahydrate (natron) or plant ash were used as fluxes by glassmakers to lower the temperature at which the silica melts. The fluxes (sodium or potassium compounds) are ionically bound into the glass network and reduce the glass viscosity, and alkaline earth metals such as calcium and magnesium are present which make the glass more durable [12,13]

Dealkalinized layers i.e., surface layers with a lower concentration of alkali and alkaline earths ions than underneath, constitute the common degradation pathology, which develops on the surface of buried glasses [6].

It is the alkali that is normally primarily lost from the glass surface upon initial corrosion [9]. In particular, ion-exchange reactions between hydrogen-bearing species of the attacking liquid and the alkali ions present in the glass take place, causing a depletion of these species in the outermost layers.

The main forms of degradation that occur are:

(i) formation on the surface of an iridescent patina that affects only the outermost layers, produced by the changed reflection conditions of the light due to the presence of the exfoliated surface [11,14–19];

(ii) formation on the surface of crusts, that make the glass opaque and determine a decrease in gloss; the alteration layers modified the surface appearance. A pearly stratification forms on the surface, which tends to fragment over time [11,20–27].

The alkaline earth metals form weak ionic bonds with the network oxygen and are replaced by  $H^+$  ions of the aqueous solution.

The first step consists of the ion-exchange of the glass alkaline ions ( $M^+ = Na^+$  and sometimes  $K^+$ ) with  $H^+$  ions from water [6].



As a consequence, within the network a depletion of alkali ions ( $Na^+$  and  $K^+$ ) and alkaline earths ions and an enrichment of hydrated silica (i.e., a layer without alkali is formed on the surface) are observable. This is a diffusive phenomenon that only involves the outermost layers and depends significantly on the composition of the glass. In general,  $K^+$  ions exchange much more easily than  $Na^+$  ions and both tend to exchange even more easily than alkaline earth ions.

The new layers formed are often brittle and can be easily detached even by small mechanical or friction impacts.

All these alterations partly result from the action of adsorbed water on the glass surfaces and partly from the deposition of other atmospheric components. In the early stages of exposure, alteration consists mainly of the crystallization of salts on the glass surface, referred to as neocrystallisations [5,7,21]. These neocrystallisations result from the reaction between the anions and the cations present in the water or in the atmosphere in the contact with the glass [5].

In a previous paper we have thoroughly investigated by means of numerous analytical techniques [28] a group of Roman and Byzantine glass shards collected during an excavation campaign at Ain Wassel in the surroundings of the ancient city of Thugga in northern Tunisia [29,30], a territory belonged to the Roman province of *Africa Proconsularis* and particularly flourishing during the Roman and Byzantine periods. The study has been carried out with the aim to chemically characterize the objects and to study the production technology including the chromophores responsible for the different color shades.

The main constituents used for ancient glass fabrication were the raw material, the flux and the coloring agents. As far as Thugga's glasses, for the raw materials a local origin of the sand has been hypothesized due to the homogeneity of the samples from the compositional point of view and in

accordance with the presence of sand deposits of important rivers of that area. Concerning the flux, in most of the cases a mixture of natron and plant ash was used [28].

With regard to the glass chemical composition, it was found [28] that the chemical elements responsible for the different glass shades were generally Fe for the green shades, copper and cobalt for the blue ones and manganese (used as discoloring agent) for the colorless samples. Roman and Byzantine glasses generally show a good standard of technology, particularly in terms of color control. Transition metal ions, such as iron ( $\text{Fe}^{3+}/\text{Fe}^{2+}$ ), cobalt ( $\text{Co}^{2+}$ ) and copper ( $\text{Cu}^{2+}/\text{Cu}^{+}$ ) acted as coloring agents.

In the present work we have investigated the degradation and corrosion products present on the surface of some of these shards. To ascertain the composition of the glass surfaces the analyses have been carried out by means of techniques such as small area XPS (X-ray photoelectron spectroscopy), SEM-EDS (scanning electron microscopy coupled with energy dispersive X-ray analysis), ATR-FTIR (Attenuated Total Reflection-Fourier Infrared Spectroscopy) and laser-ablation ICP-MS (Inductively Coupled Plasma-Mass Spectrometry).

## 2. Materials and Methods

The investigated samples belong to the small finds of the University of Trento's excavation of the Late Antique-Byzantine farm at Ain Wassel (or Ouassel) in Northern Tunisia (ancient Africa Proconsularis), carried out between 1994 and 1996. The vast site is located at 530 m asl on the southern slope of a hill, in the surroundings of the well-known city of Thugga. During fieldwork, 132 glass fragments have been collected, representing approximately 1% of the discovered archaeological material. The shards could be associated with 56 different glass forms or objects, partly dating to the late 4th and 5th century A.D. and partly to the 6th and 7th century A.D. [29,30] In this work some samples belonging to stemmed goblets and to a toed lamp from the latter period have been selected and are reported in Table 1 and Figure 1. All the glasses presented, on the surface, some areas where evident alterations were present. The analytical techniques employed for the characterization of each sample are also listed.

**Table 1.** Analyzed glass samples: together with the color, the analytical techniques employed for the characterization of each sample, are here listed.

Sample Identification	Color	Analytical Techniques
GLR011 (sample n.24 in [28])	light yellow	SEM-EDS, small-area XPS
GLU034 (R14-U209, not included in [28])	light blue	SEM-EDS, LA-ICP-MS
GLB002 (sample n.39 in [28])	colorless-light blue	SEM-EDS, FT-IR, small-area XPS, LA-ICP-MS
GLR014 (sample n.22 in [28])	yellowish	SEM-EDS, small-area XPS

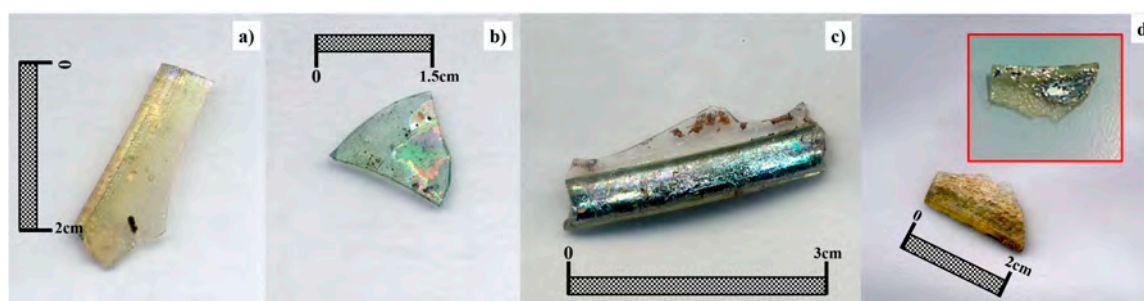


**Figure 1.** Samples GLR011 (a) and GLU034 (b) and GLB002 (c) and (d) GLR014 showing typical degradation layers. The names of the fragments are the first ones assigned after the excavation: they indicate the material glass GL, and the type of fragment referred to a shape (B base, R rim, U unidentified).

### 2.1. Small-Area XPS (Small-Area X-ray Photoelectron Spectroscopy)

Small-area XPS was performed on selected regions of the sample surface using a monochromatic and focused Al  $K\alpha$  X-ray source to determine the elemental chemical composition, the chemical state of the elements and the atomic concentration. The analysis areas were chosen using a microscope mounted on the ultrahigh vacuum chamber and the images were saved together with the XP-spectra. The X-ray spot was of 400  $\mu\text{m}$  and the pass energy was set at 100 eV for the high-resolution spectra and at 200 eV for the survey ones. Under these conditions the full width at half maximum of Ag  $3d_{5/2}$  recorded on sputtered silver was found to be 0.83 eV when the pass energy was set at 100 eV. A flood gun was used for charging compensation and the binding energy scale was referenced to the adventitious aliphatic at 285.0 eV. More details on experimental set up and data processing are provided in [28].

### 2.2. SEM-EDS (Scanning Electron Microscopy Coupled with Energy Dispersive Spectroscopy)

The glass shards were analyzed by SEM-EDS to obtain qualitative/semiquantitative information on the chemical composition in both unaltered and altered areas. The analyses have been acquired using the ZAF (Z = atomic number; A = self-absorption effect; F = fluorescence effect). During this procedure the data are automatically normalized. For each analysis 3 measurements were performed. The instrument employed was a Hitachi TM1000 equipped with an energy dispersive X-ray spectrometer (Oxford Instruments SwiftED). The images have been acquired at different magnifications while EDS analyses were performed on areas of about  $300 \times 300 \mu\text{m}$ . Measurements were directly performed on samples since no metal coating was required according to a procedure previously set up [31].

### 2.3. ATR-FT-IR (Attenuated Total Reflection-Fourier Infrared Spectroscopy)

Infrared spectra were collected on the micro samples by a Nicolet 380 spectrophotometer coupled with ATR accessory Smart Orbit equipped with a diamond crystal. Spectra have been acquired in the range  $500\text{--}4000 \text{ cm}^{-1}$  at a resolution of  $4 \text{ cm}^{-1}$ .

### 2.4. LA-ICP-MS (Laser Ablation Inductively Coupled Plasma Mass Spectrometry)

Trace element concentrations were measured using an Inductively Coupled Plasma Mass Spectrometry with Laser Ablation (LA-ICP-MS). The LA-ICP-MS equipment was an Elan DRc (Perkin Elmer/SCIEX), connected to a New Wave UP213 solid-state Nd-YAG laser probe (213 nm). Samples were ablated by laser beam in a cell, and the vaporized material was then flushed (Gunther & Heinrich 1999) [32] to the ICP, where it was quantified. The procedures for data acquisition were those normally used in the Mass Spectroscopy Laboratory of the Department of Biology, Ecology and Earth Sciences, University of Calabria [33–36].

Two different types of analyses were executed on each fragment. Using an ablation crater of 50  $\mu\text{m}$  in diameter and 70/80  $\mu\text{m}$  in depth, three/four spot analyses were carried out on each shard to determine the trace elements composition.

Then the analyses were executed along an ablation line characterized by a length of about 50  $\mu\text{m}$  and a depth and a width of 5  $\mu\text{m}$ , to determine the trace elements composition of degraded areas and to be sure to analyze only the degraded layer. In both cases the ablation time was about 60 s.

## 3. Results

### 3.1. SEM-EDS

Electron microscopy, in combination with energy dispersive X-ray microanalysis, has successfully contributed to the investigation of degradation phenomena on materials of art and archaeology [37–39]. In the present study SEM-EDS investigations made it possible to highlight mainly two kinds of surface degradation developed on the different samples, i.e., iridescent patinas and crusts.

In Table 2 the results of SEM-EDS analysis on samples GLU034, GLR011 and GLB002 are reported. GLU034 and GLR011 samples (Figure 2) appear iridescent in the altered areas. The results of elemental analyses for sample GLR011 are shown also in Figure 3 to better evidence the differences between unaltered and altered area. In the altered areas an enrichment in silica and a depletion in alkali is observable. It is worth nothing that, as already reported in our previous work dealing with the characterization of these glasses [28], low sodium concentrations were generally detected, but this is in accordance with other cases reported in the literature as we have already underlined in Fermo et al. 2016 [28]. This has been observed for all the samples and it could probably be attributable to some initial depletion in sodium even if visually unaltered areas are clearly observable, as is well evident from the images reported in Figure 1.

**Table 2.** SEM-EDS semi-quantitative analyses (wt%); for each oxide and element, the percentage is calculated as mean value over three measurements on two different areas of the same sample; for all the detected elements and oxides the standard deviation was lower than 5%.

	GLU034		GLR011		GLB002	
	Unaltered Class	Altered Glass Iridescent Patina	Unaltered Glass	Altered Glass Iridescent Patina	Unaltered Glass	Altered Glass External Crust
Na <sub>2</sub> O	2.88	2.24	2.26	1.85	2.44	3.24
MgO	1.62	0.56	0.22	-	0.67	1.70
Al <sub>2</sub> O <sub>3</sub>	1.00	5.82	6.48	7.54	3.32	5.64
SiO <sub>2</sub>	75.68	73.17	66.41	76	81.05	42.00
CaO	9.06	9.26	13.32	8.44	6.45	7.98
K <sub>2</sub> O	4.69	5.42	5.44	1.90	2.70	3.19
TiO <sub>2</sub>	1.93	0.84	1.37	1.11	0.00	2.00
Fe <sub>2</sub> O <sub>3</sub>	1.31	0.90	2.54	1.58	1.60	8.98
MnO	0.57	0.73	-	-	0.00	24.02
Cl	1.25	1.05	1.96	1.58	1.78	1.32
S	-	-	-	-	-	1.20

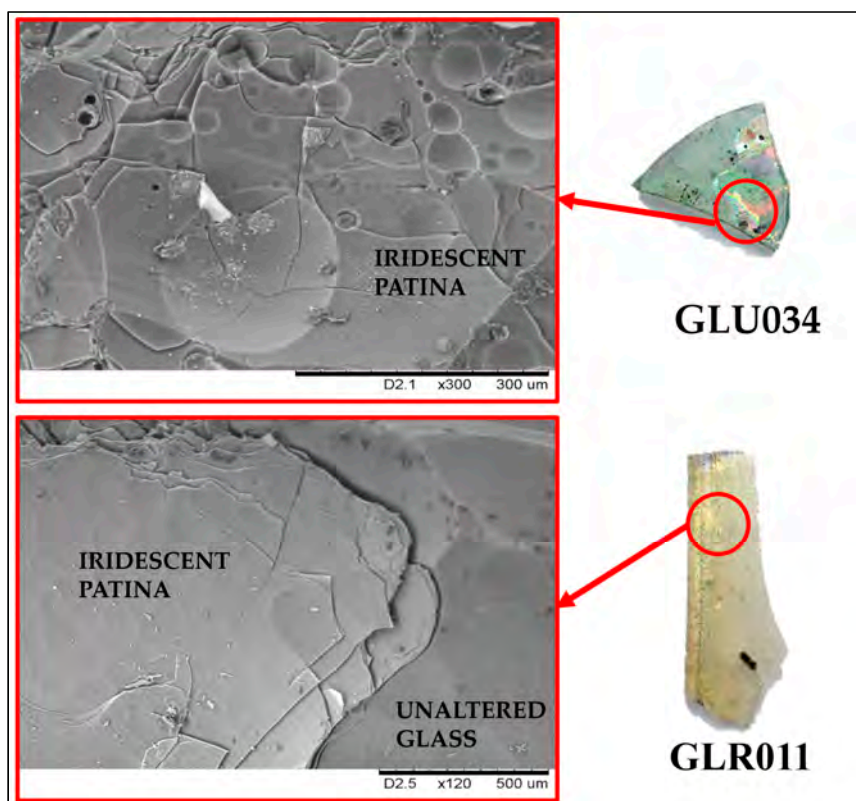


**Figure 2.** SEM images acquired on the iridescent surface of GLU034 and GLR011 samples.

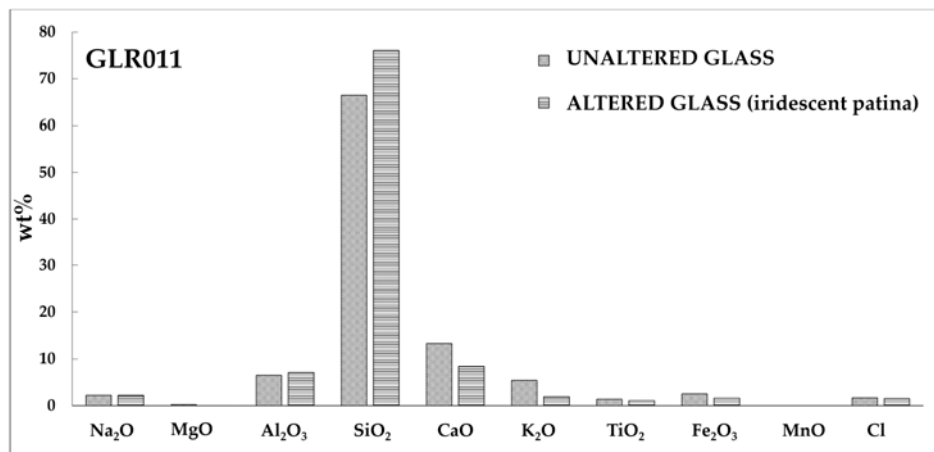


**Figure 3.** Mean concentrations (wt%) detected by SEM-EDS of the elements present on the altered (iridescent area) and unaltered area of sample GLR011.

The alteration phenomenon that we have observed, i.e., iridescent patina and crusts formation on the surfaces of our samples, have been already observed in the literature (see also the description reported in the introduction) [11,20–27,40–42].

A different situation has been observed for sample GLB002 (Figure 4) with respect to what was observed for samples GLR011 and GLU034; it showed on the surface a layer of dark brown encrustations (an iridescent area was also present in this sample, but it was not possible to analyze it by SEM-EDS because of the poor quality of the signal, due to the orientation of the surface/electron beam). For sample GLB002 a depletion in silica and an enrichment in alkali is present (Figure 5). Furthermore, the black encrustations are enriched in titanium, iron and manganese. It is worth noticing that these elements are those typically present in the glass composition [28].

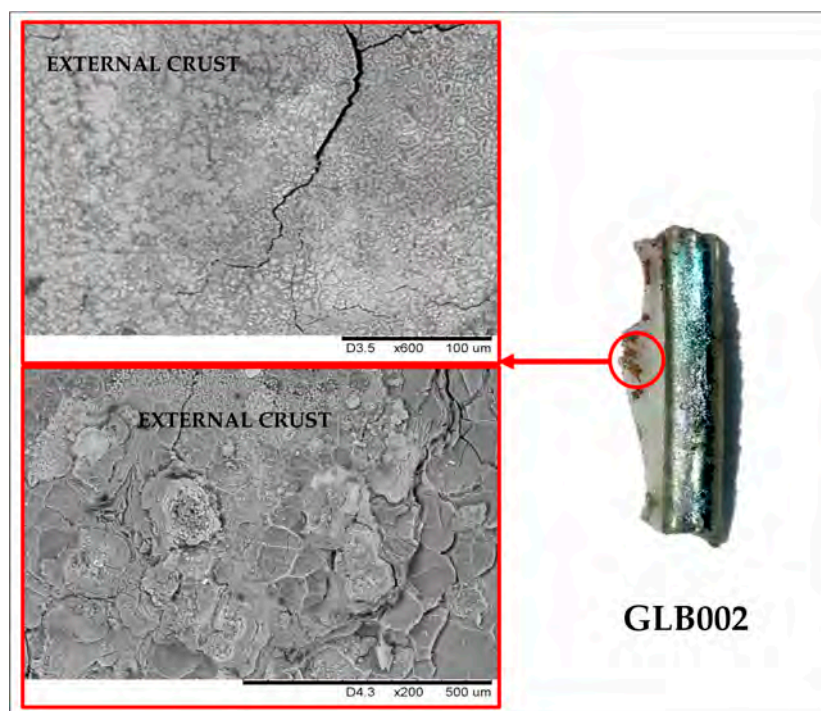


**Figure 4.** SEM images acquired on the dark-brown area of sample GLB002.

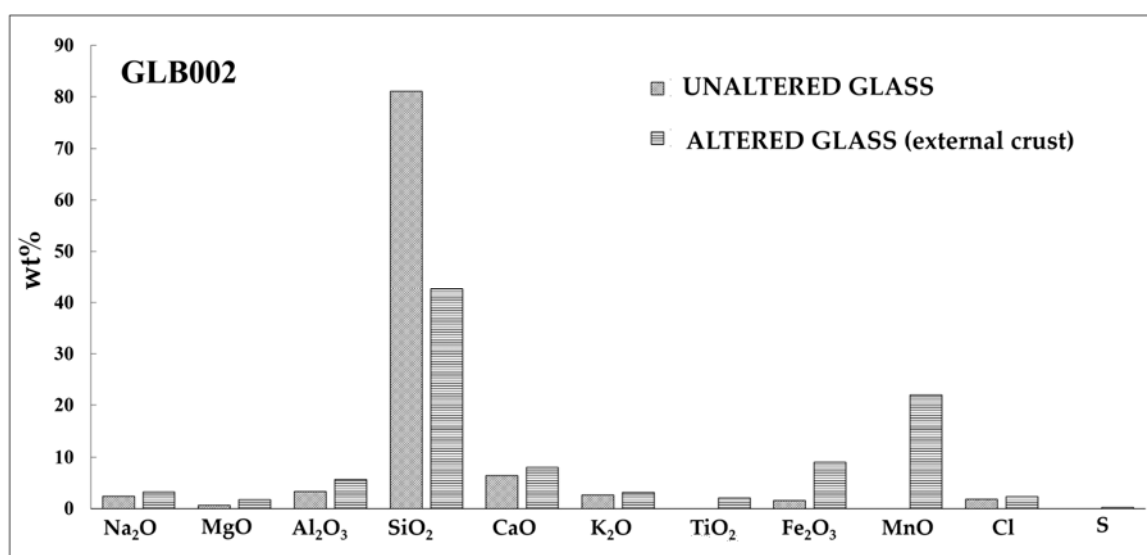


**Figure 5.** Mean concentrations (wt%) detected by SEM-EDS of the elements present on the unaltered and altered areas (showing the presence of a crust) of sample GLB002.

### 3.2. FT-IR

ATR-FTIR was used for investigating the incrustations present in the altered areas. As an example, in Figure S1 (Supplementary Material) the spectra acquired on various regions of sample GLB002 are reported. The typical signals due to CaCO<sub>3</sub> at about 1420 and 871 cm<sup>-1</sup> are present together with some signals of lower intensity at about 2920 cm<sup>-1</sup> attributable to organic substances (probably due to some contamination from the soil) while at about 1000 cm<sup>-1</sup> there is the stretching of Si-O-Si functionality. The broad band between 3600–3400 cm<sup>-1</sup> was attributed to some water probably absorbed on the surface.

### 3.3. Small Area XPS

Samples labeled GLR014, GLB002 and GLR011 were selected for the present investigation since they show various kinds of weathering: iridescence and incrustations. X-ray photoelectron spectroscopy, which is a non-destructive technique, may be operated in various modes and within them small-area XPS was selected in the present investigation. The reason for this choice is that, despite a decrease in the signal intensities, this technique allows the gaining of chemical information only of the altered regions as well of the regions that morphologically exhibit changes in color or the presence of deposits, provided that the analyzed region is at least three times larger than the beam diameter selected for the analysis. In this way, it is possible the characterization of selected regions of the sample and thus a comparison of the composition between morphologically different areas for obtaining information is useful in the identification of the degradation process.

Through XPS the surface concentrations of the main chemical elements have been obtained and, in particular, the oxidation states of the elements, the presence of carbonate salts and concentration trends of some elements in the outermost layers.

As far as GLB002 sample, three different regions were characterized, as pointed out in the photographs of Figure 6: point 1 in Figure 6a, external crust labeled as point 2 in the same figure and an iridescent area (point 3 in Figure 6a).

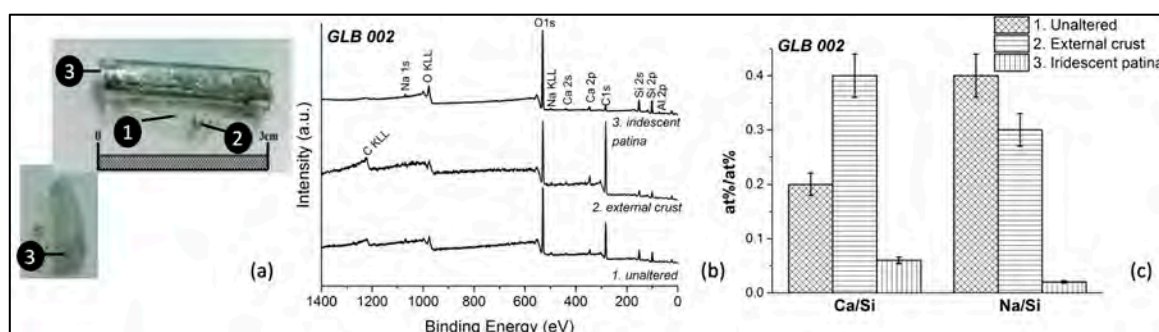


**Figure 6.** (a) The pictures show the analyzed areas in sample GLB002; (b) It reports X-ray photoelectron survey spectra acquired on the three different areas with a monochromatic Al  $K\alpha$  X-ray source; and (c) compares the surface cations-to-silicon ratios.

A detailed inspection of the survey spectra (Figure 6b) allows the identification of the main constituents of the samples' surfaces. Oxygen, silicon, aluminum, calcium and sodium were detected on the surfaces of all the analyzed areas. Potassium was only revealed in point 1 and small amounts of iron were found on the external crust (point 2) and on the iridescent portion of the sample (point 3) (Figure 7). A curve fitting of Fe 2p peaks according to [43] was performed and allowed the observation that in the external crust the % of the peak area ascribed to Fe (II) is lower (13%) than in the iridescent areas (35%).

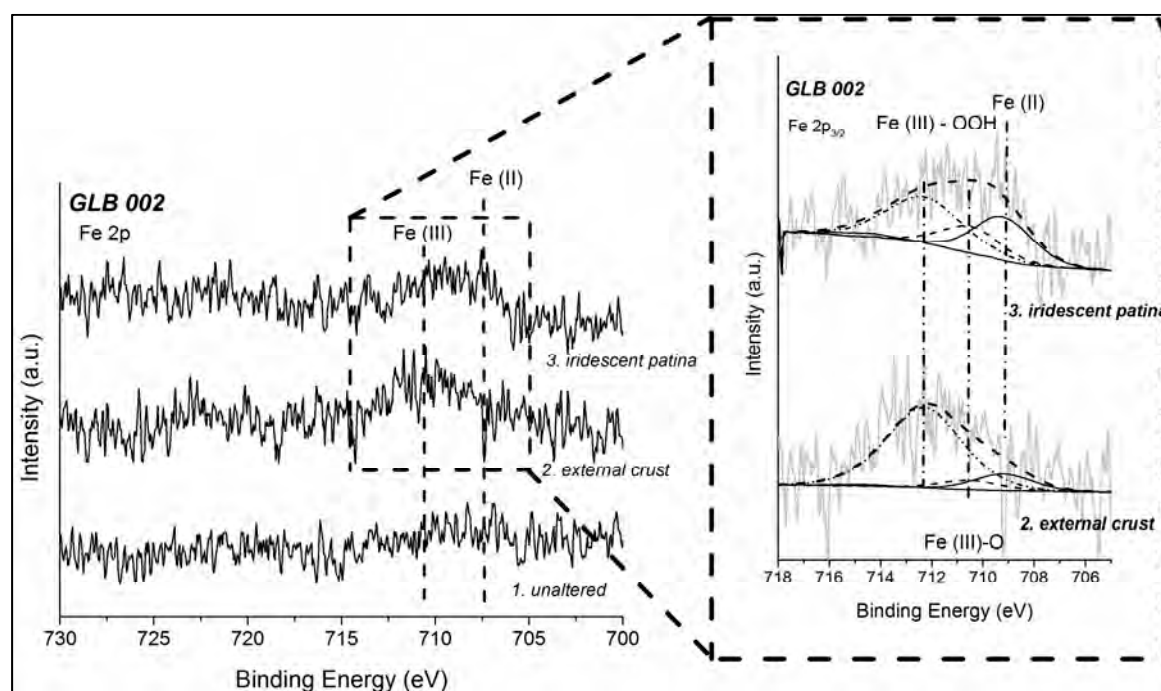


**Figure 7.** Fe 2p peak obtained on the sample GLB002 in point 1, in the external crust (point 2) and in the iridescent patina (point 3).

Surface composition is given in atomic percentage (Table S1). The external crust and the iridescent patina were clearly depleted in alkali: K is not detected in point 2 and 3 and Na/Si ratio decreases from 0.3 in point 1 to 0.2 in the external crust, and it is found to be 0.03 in the iridescent patina (point 3 Figure 6c). Ca/Si ratio is higher in the external crust than in the point 1 while it is lower in the iridescent patina.

Two different regions were analyzed in the GLR011 sample: point 1 (unaltered) and point 2 (iridescent patina) in Figure 8a.

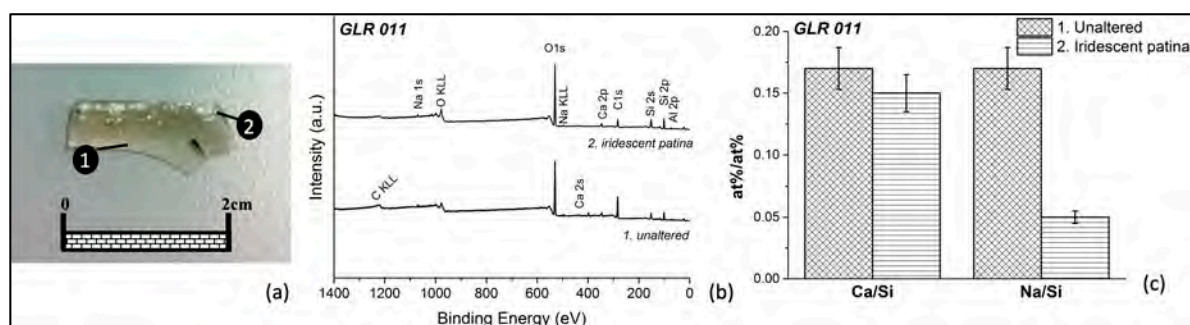


**Figure 8.** (a) The analyzed areas selected on sample GLR011 are shown in the photograph; (b) The X-ray photoelectron survey spectra acquired on the two different areas with the monochromatic Al K $\alpha$  X-ray source using a beam of 400  $\mu$ m are compared and (c) the chemical composition provided as surface cations/silicon ratios is presented for the same analysis points.

The detailed surface composition in atomic percentages of the GLR011 sample is reported in Table 2. Si, O, Al, Ca and Si were the only detectable elements together with C. The presence of this element might be ascribed to contamination (Figure 8b). The cations-to-Si ratios showed a pronounced depletion of Na (Figure 8c) in point 2, which exhibits an iridescence compared to point 1 and a minor decrease of the Ca/Si ratio.

Also, in the case of sample GLR014 two different areas were characterized, i.e., point 1 and point 2 of Figure 9a.

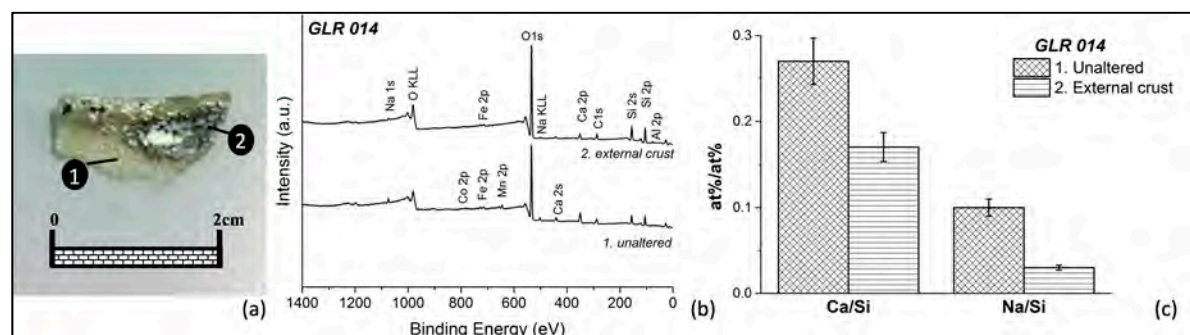


**Figure 9.** (a) The analyzed areas in sample GLR014 show the regions where the XPS spectra were collected; the corresponding X-ray photoelectron survey spectra acquired on the two different areas with a monochromatic Al K $\alpha$  X-ray source are shown in (b) together with the surface cations-to-silicon ratios (c).

The inspection of the survey spectra acquired on sample GLR014 allows the identification of iron, cobalt and manganese together with oxygen, silicon, aluminum, sodium and calcium in point 1 of this sample (Figure 9b); Table 2 lists the atomic percentages and Figure 9c shows the atomic ratios. (Table 2 and Figure 9c). Cobalt and manganese were not detected in point 2, which is iridescent. Some significant marked differences are better revealed by the high-resolution XP-spectra for the different analyzed points on this sample.

The first one involves the Fe 2p peak, which showed a different distribution of Fe (II) and Fe (III) in the two points (Figure 10a). In point 1 the Fe (II) component is more pronounced than in the altered one (point 2); in the altered area on the contrary the iron oxy-hydroxide component is the most abundant Fe species. This finding is substantiated by the O 1s peak, which showed a marked difference on its components in the different points (Figure 10 b). O 1s is a multicomponent peak: the signal at 530.2 eV is due to oxygen in oxides, the one at 531.5 eV is assignable to –OH [43] and to non-bridging oxygen in silicates, and the component at the highest binding energy values (532.3 eV) is ascribed to bridging oxygen in silicates. In point 2, the second component is the most intense, confirming the larger presence of –OH in this area than in the unaltered one. The most intense photoelectron signal

assigned to Mn2p also allows the identification of the chemical state of this element, which is found to be Mn<sup>4+</sup> (see Figure S2 in supplementary information).

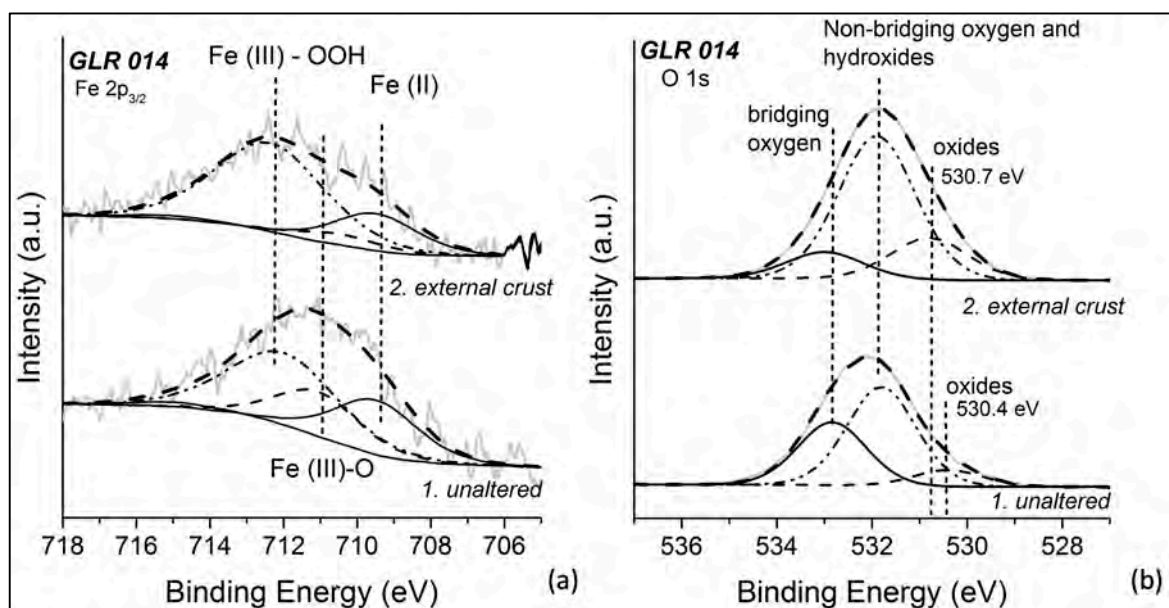


**Figure 10.** Fe 2p<sub>3/2</sub> peaks recorded points 1 and 2 of sample GLR 014 (a and b respectively) as well as the O 1s peaks recorded in of sample GLR 014 (a and b respectively).

Another impressive difference is related to the carbon components: carbon is always present in all the samples in contact with the atmosphere, as an organic contamination layer. In point 1, C 1's peak showed an intense peak due to carbonate (Figure S3a); the intensity of the component dramatically decreases in point 2 (Figure S3b).

### 3.4. LA-ICP-MS

Two samples (GLB002 and GLU034) were analyzed by LA-ICP-MS with the aim of obtaining the trace elements concentrations (Table 3). For both of them, the analyses were carried out in spot and linear modality (see Materials and Methods paragraph).

**Table 3.** Average concentration resulted from four analyses by LA-ICP-MS (expressed in ppm) of the most representative chemical elements, both on unaltered and altered glass for samples GLB002 and GIU004 samples.

	GLB002		GLU004	
	Unaltered Glass	Altered Glass	Unaltered Glass	Altered Glass
Ti	698	2927	831	561
Mn	9398	19914	518	246
Co	6	27	5	11
Co	6	27	5	11
Cu	24	-	-	-
Cr	121	23	36	32
Ni	11	211	5	6
Pb	15	150	11	68

Among all analyzed elements, Co, Mn, Pb and Ti are the most significant. In particular, comparing the concentrations of altered areas with those measured on the unaltered glass, sample GLU034 shows similar Co concentrations in both portions (iridescent patina and unaltered glass), a decrement of Mn

and Ti and an increase of Pb from unaltered glass to iridescent patina. The black encrustation of the GLB002 sample, instead, exhibits an enrichment in Co, Mn, Pb and Ti.

#### 4. Discussion

It is acknowledged that ancient glasses exposed for long time to unfavorable conditions undergo transformations and alterations. The degradation processes strongly depend on the chemical composition and environmental parameters of the glasses (such as soil humidity, temperature and pH). Exchange reactions take place between the so-called network modifier ions ( $\text{Na}^+$ ,  $\text{K}^+$ ,  $\text{Ca}^{2+}$  and  $\text{Mg}^{2+}$ ), added to the raw materials in the form of oxides or carbonates to decrease the melting point and making the glass more resistant towards chemical attack and water [37].

It has to be noticed that this study area in Northern Africa is subject to the semi-arid Mediterranean climate with few rainfalls, although the site of Ain Wassel in the Arkou valley has a sub-humid microclimate. Soils are in general clayey, but permeable enough. Worth noting in the region is the presence of salt, originating from the weathering of local diapiric structures, which partly erodes the land surface [44,45].

Systematic studies on the corrosion of glasses, i.e., the attack of aqueous solutions onto the glass surface, have been often carried out in the literature by means of SEM-EDS [37]. This technique has allowed us to highlight morphological and elemental distribution differences between altered and unaltered areas. In the case of iridescent regions an increase of Si and alkali depletion was detected (see samples GLR011 and GLU034).

The weathered glass is a complex system characterized by the presence of very fragile multilayered silica, where the number of layers and their thickness depend upon time. The weathering is mainly due to the effect of water that, through the mechanisms of diffusion and ionic exchange, produces a general loss of modifier ions on the surface of glass, generating almost pure silica iridescent layers [46] like those observed for samples GLR011 and GLU034. In general, three different layers can be identified in weathered glasses: the unaltered bulk glass, the gel layer composed by a hydrated silica network (typically, samples GLR011 and GLU034) and the layer of corrosion salts externally formed (GLB002).

Samples GLU034 and GLR011 (Figure 2) show the characteristic lamellar structure formed following the leaching process of alkali ions. Elemental analysis of altered and not altered surfaces, carried out by SEM-EDS analysis on these samples, has shown that the degraded surface is characterized by alkali depletion and an increase in silica, compared to less unaltered surface. This ion exchange causes the formation of a thin layer near the glass surface, which is relatively enriched in silica and contains a low amount of other cations.

Alkaline-earth ions ( $\text{M}^{2+}$ ) could also leach out by a similar mechanism. Indeed, often the leaching of Na from soda-silica-lime glass results in the formation of an outer so-called gel layer, mainly consisting of the remaining glass components ( $\text{SiO}_2$  and CaO) [47]. Curious growth rings develop on the surface of the glass. This characteristic phenomenon has been observed for sample GLU034 (Figure 2). The alteration layer shows the presence of flakes (Figure 2): in fact, cracks form as the degradation increases, and they become a vehicle for the passage of water for a subsequent attack.

The leaching phase is followed by a corrosion process in which the silicon oxygen bonds (Si-O-Si) are broken. This phenomenon is called glass depolymerization and progresses gradually to greater depths up to 150  $\mu\text{m}$ .

Cracks have been clearly observed for samples GLU034 and GLR011. In particular, in sample GLU034, the presence of craters highlights the beginning of the corrosion process. Many authors describe that the transition from the degradation phase, defined as leaching to the corrosion phase, can be highlighted on the surface by observing these typical craters; in fact, over time they tend to widen (as the degradation proceeds) until their complete interconnection [10,14,16,18,23].

The layers produced are fragile and inconsistent and this leads to the thinning of the surface. As degradation proceeds, new effects are produced on the surface, which are formed by interaction with pollutants and carbon and sulfur dioxide, which cause the precipitation of salts on the surface.

Some weathering products can be observed on the glass surface in accordance with what is reported in the literature [37]. In particular in our case the presence of  $\text{CaCO}_3$  has been observed by ATR FTIR (Figure S1) together with traces due to organic substances (signals at about  $2920\text{ cm}^{-1}$ ) in accordance with what described by Schreiner et al. [37] where it is reported that the weathering product could be calcium carbonate or some organic Ca-containing compound.

The development of corrosion crusts complicates the analysis of historical glass pieces and the diagnosis of their deterioration [4].

Contrary to the iridescent areas, where a leaching of alkali and alkaline earth ions causes the modification of the glass network, browning corrosion is due to the migration of Mn, Fe and other metallic ions carried by the attacking aqueous solution, which enter in the glass from the surrounding soil or are depleted from the pristine glass core (this is the case of Mn and Fe) [46]. This is perfectly in accordance with what observed for sample GLB002 where an enrichment mainly in Mn, Fe and Ti has been observed on the encrustations together with an increase in Ca, K, Na, Mg, Al, Cl and S (Figure 5). In this case different compounds could be formed; for example, in the literature Fe (III) oxide and oxide hydrates, insoluble sulfides or manganese dioxide are reported and are in part responsible for the darkening of the glass [3]. Nevertheless on the base of elemental analysis by SEM-EDS, it is difficult to make hypotheses on the chemical nature of the species present on the surface. We can just presume that, for example, the observed increment on the encrustations of S, K, Ca, Na and Cl concentrations in case of sample GLB002 could be due to the formation of sulphates such as syngenite ( $\text{K}_2\text{SO}_4 \cdot \text{CaSO}_4 \cdot \text{H}_2\text{O}$ ) or of chloride as NaCl in accordance to what is observed by Schreiner et al. [37].

From the point of view of the surface morphology, sample GLB002 shows (Figure 4) the typical features characteristic of corrosion processes [48].

XPS has been already applied in the literature for the characterization of the alteration and corrosion phenomena occurring in Roman glass fragments [49] and for investigating the weathering process of glass surfaces with the formation of corrosion growth rings detected by optical microscope [46].

A comparison has been carried out between EDS and XPS results (Figure 11) in order to highlight differences in the chemical composition of the outermost layers compared to the bulk. To this purpose Ca/Si and Na/Si ratios have been considered (atomic percentages detected by XPS were converted into weight percentage in order to compare the results). For sample GLR011 it is confirmed also for the outermost layer what was already observed for the bulk, i.e., a decrease of both Ca/Si and Na/Si ratios in the altered areas confirming the formation on the surface of a silica gel depleted in alkali ions.

The formation of silica gel is confirmed by XPS data: taking into account all the samples, the binding energy of Si 2p increases with sodium and calcium depletion towards values typical of  $\text{SiO}_2$  (Figure 12a). Besides, in O 1s peaks, the component ascribed to non-bridging oxygen increases its intensity in the visibly altered regions, where cation/silicon ratios decrease (Figure 12b). If the non-bridging/bridging oxygen area ratio (NBO/BO) is plotted *vs* Ca/Si (Figure 12c) and Na/Si (Figure 13) ratios it is evident that, in the cation depleted areas, NBO/BO increases substantiating the hypothesis of silicate depolymerization. The only exception is represented by point 2 of the GLB002 sample where NBO/BO increases with the Ca/Si ratio (Figure 12c). In that area encrustations enriched in  $\text{CaCO}_3$  have been evidenced: XPS analysis has highlighted how Ca enrichment takes place in the outermost layer (Ca/Si ratio determined by XPS is remarkably higher than that determined by EDS) and the presence of calcium carbonate is in agreement with the FT-IR spectra.

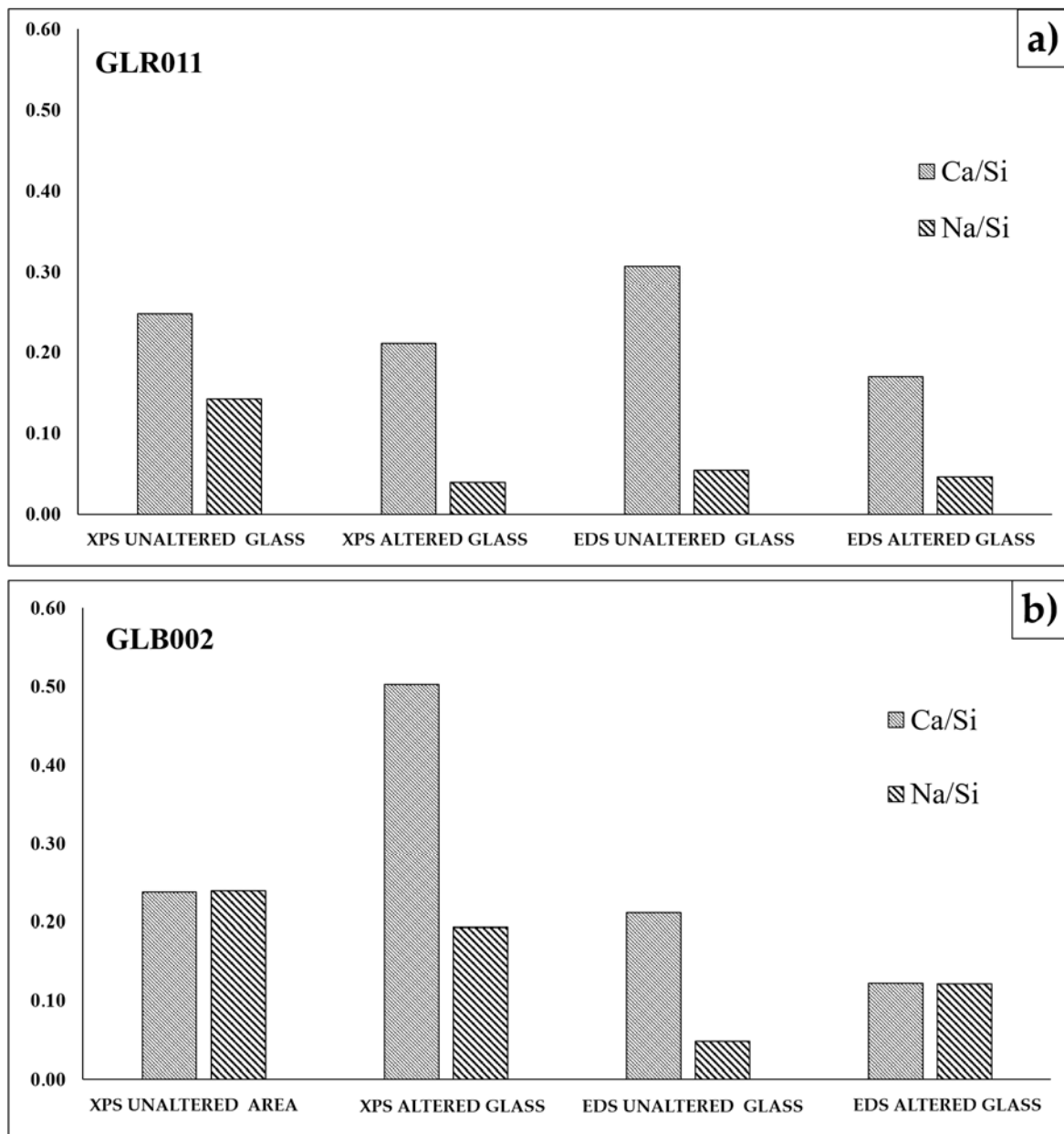


**Figure 11.** Ca/Si e Na/Si ratios obtained from XPS and EDS analyses carried out on unaltered and altered glass areas for samples GLR011 (a) and GLB002 (b).

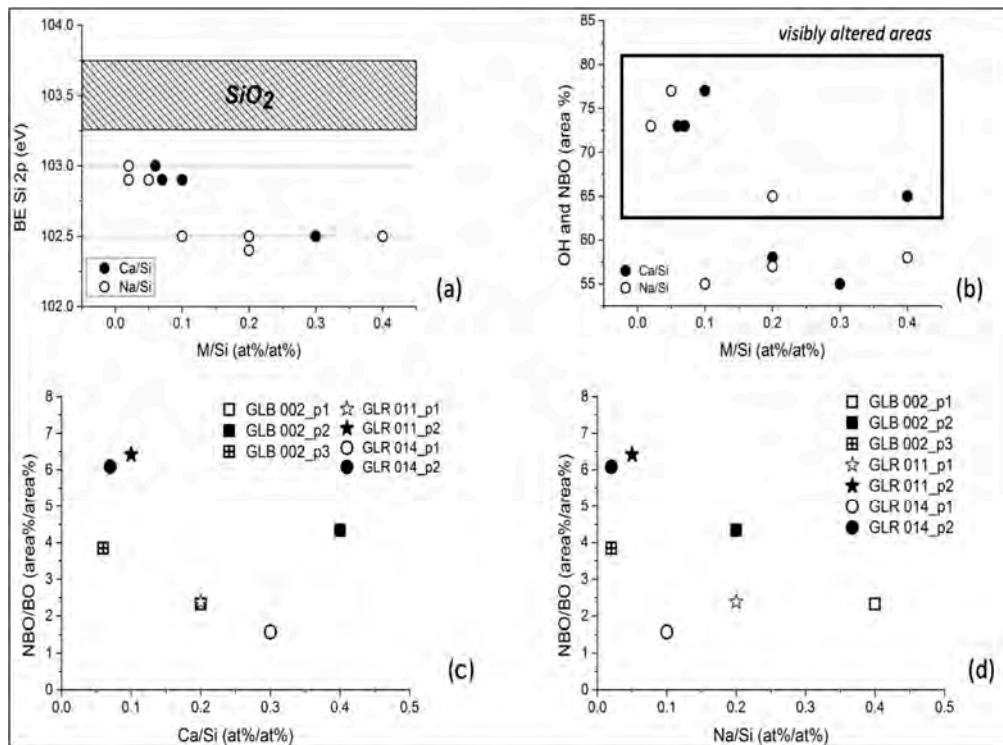


**Figure 12.** (a) binding energy (BE) of XPS Si 2p peak versus cation/Si ratios. The shaded area represents the range of BE reported in literature for SiO<sub>2</sub>. [50] [ref: <https://srdata.nist.gov/xps/selEnergyType.aspx>]; (b) Area % of non-bridging and OH component in O 1s peak vs Ca/Si and Na/Si ratios; (c) non-bridging/bridging oxygen area ratio from O 1s peaks vs Ca/Si ratios and (d) Na/Si ratios.

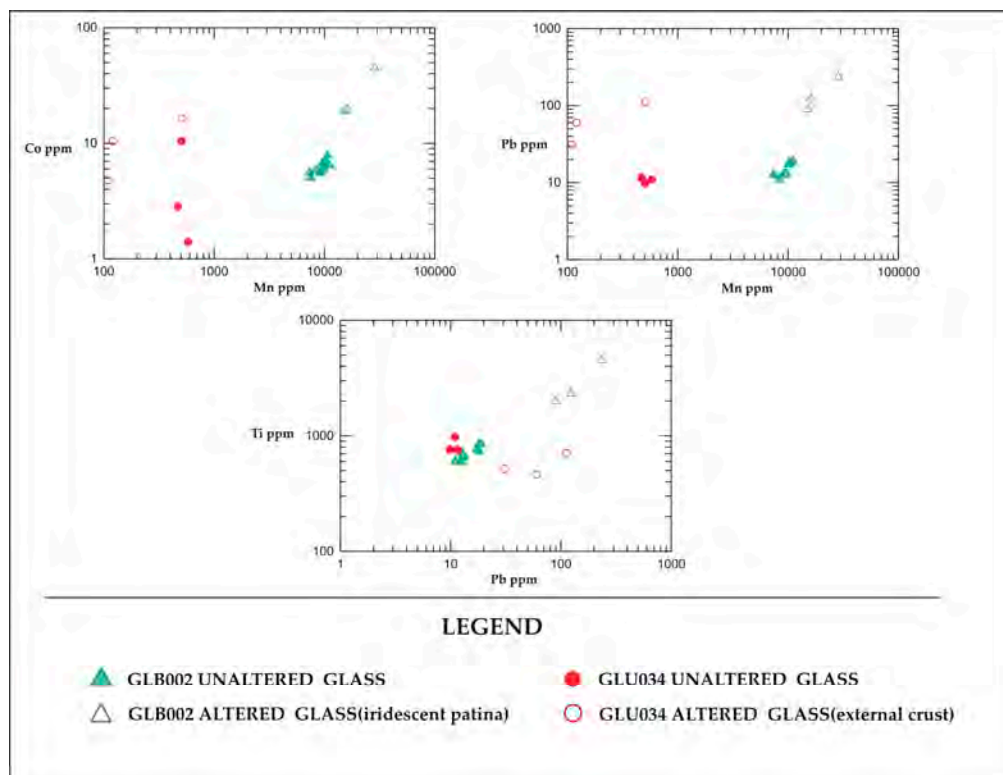


**Figure 13.** Binary diagrams relative to the concentrations of some trace elements such as: Co vs Mn, Pb vs Mn and Ti vs Pb, detected on different morphological glass areas.

It is worth noting that also Fe 2p signals recorded in the visibly altered regions of samples GLB002 and GLR014 reflect the higher amount of hydroxides, whose signals in O 1s peaks fall at the same binding energy values of NBO, being the components at about 712 eV more intense in the external encrustations (points 2).

As far as sample GLR014, the presence of an intense component ascribed to carbonate in C 1s signal recorded on point 1, could be due the presence of sodium and calcium carbonate. The marked decrease of sodium, calcium (and also of other metals such as Co and Mn) and of the carbonate component in point 2 could be due to leaching processes.

The LA-ICP-MS results highlight the different enrichment patterns observed in the black encrustation of GLB002 and in the iridescent patina of GLU034. Indeed, the black encrustation of GLB002 compared to the unaltered bulk glass is always enriched in Co, Mn, Ni, Pb and Ti. It is worth mentioning that Mn and Ti enrichment was also confirmed by SEM-EDS data. Enrichment in Mn has also been observed on encrustations in another study reported in the literature [40].

The iridescent patina of GLU034 sample, compared to the unaltered bulk glass, only shows a higher value of Pb.

Considering that the Pb is calcium-vicariant, his enrichment is coherent with the observed presence of Ca compounds in both samples. Moreover, the higher values of other heavy metals (Co, Ni, Ti) are in agreement with the presence of different compounds (oxide and oxide hydrates, insoluble sulfides or manganese dioxide) and they are jointly responsible for the darkening of the glass [49].

The different chemical behavior of the two types of degradation layers is evident in the binary diagrams Co versus Mn, Pb versus Mn and Ti versus Pb (Figure 13) and in the histograms of Figure 14. The black encrustation of GBL002, instead, is depleted in Cu and Cr. Since the investigations have been performed only on a limited number of samples, advancing explanations for these phenomena might be speculative. Nevertheless, the increase in some elements such as Pb on the altered areas could be explained with depletion in other elements.

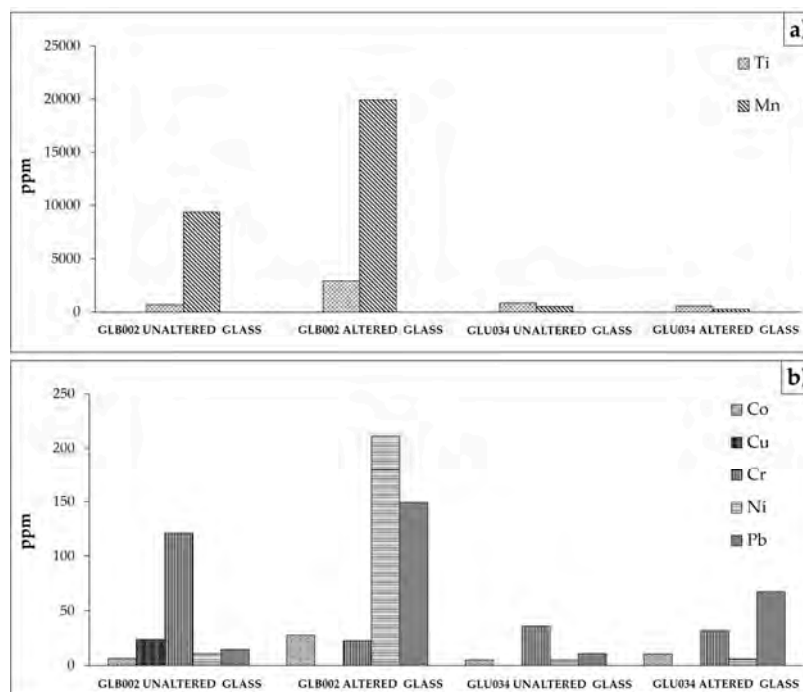


**Figure 14.** Histograms of (a) Mn, Ti; (b) Co, Cr, Cu, Ni, Pb in both unaltered and altered areas of GLB002 and GLU034 samples.

## 5. Conclusions

The present paper is focused on the characterization of the degradation products present on the surface of some Byzantine glass shards. The surface of the investigated samples appears to be differently altered: where alkali depletion occurred together with enrichment in silica the appearance of iridescence is very pronounced in the most damaged areas. On the other hand, the enrichment in Ca or in some other metals, such as Mn, was revealed in the case of the encrustations. The applied techniques allowed the identification of the morphology of the differently altered regions on the same sample as well as the elemental composition of the bulk by SEM-EDS. The information obtained by XPS is complementary: the outermost surface and the compounds present in the various points have been fully characterized. A technique such as LA-ICP-MS is demonstrated to be particularly useful for quantifying metal in trace amounts and for discriminating the two kinds of degradation phenomena on the base of some binary diagrams.

**Supplementary Materials:** The following are available online at <http://www.mdpi.com/2076-3417/10/21/7523/s1>, Table S1: Quantitative composition in atomic percentage of the surface of all samples considered in this investigation is here presented. The composition of the various points is also listed. Accuracy is estimated to be  $\pm 10\%$ . Figure S1: ATR IR spectra obtained on degraded glass regions (green and blu solid lines) and on unaltered glass (red line) for sample GLB002, Figure S2: Mn  $2p_{3/2}$  peaks recorded in point 1 of sample GLR 014. The chemical state of Mn, determined taking into account the multiplet structure of core p- vacancy levels [Gupta, R.P. and Sen, S.K. (1975), Calculations of multiplet structure of core p-vacancy levels. *Physical Reviews B*, 10, 71–79], was found to be  $Mn^{4+}$ , Figure S3: C 1s peaks recorded in point 1 and in point 2 of sample GLR 014 (a and b respectively).

**Author Contributions:** Conceptualization, P.F. and V.C.; methodology, V.C., A.R., M.F., D.A.; investigation, V.C., M.F., D.B.; data processing, P.F., A.R., M.F., V.G., D.B., M.F.L.R.; writing—original draft preparation, P.F., V.C., A.R., M.F.; writing—review and editing, P.F., A.R., M.F., V.G., D.A., M.F.L.R.; supervision, P.F., A.R., M.A.; project administration, P.F.; All authors have read and agreed to the published version of the manuscript.

**Funding:** This research was partially funded by University of Cagliari and partly by the University of Milan.

**Conflicts of Interest:** The authors declare no conflict of interest.

## References

1. Barbera, G.; Crupi, V.; Longo, F.; Majolino, D.; Mazzoleni, P.; Venuti, V. Study of Late Roman and Byzantine glass by the combined use of analytical techniques. *J. Non-Cryst. Solids* **2012**, *358*, 1554–1561. [[CrossRef](#)]
2. Huisman, D.J.; Pols, S.; Joosten, I.; Van Os, B.J.H.; Smit, A. Degradation processes in colourless Roman glass: Cases from the Bocholtz burial. *J. Archaeol. Sci.* **2008**, *35*, 398–411. [[CrossRef](#)]
3. Doménech Carbo, M.T.; Doménech Carbò, A.; Osete Cortina, L.; Sauri Peris, M.C. A Study on Corrosion Processes of Archaeological Glass from the Valencian Region (Spain) and its Consolidation Treatment. *Microchim. Acta* **2006**, *154*, 123–142. [[CrossRef](#)]
4. Carmona, N.; Oujja, M.; Rebollar, E.; Romich, H.; Castillejo, M. Analysis of corroded glasses by laser induced breakdown spectroscopy. *Spectrochim. Acta A* **2005**, *60*, 1155–1162. [[CrossRef](#)]
5. Gentaz, L.; Lombardo, T.; Chabas, A.; Loisel, C.; Verney-Carron, A. Impact of neocrystallisations on the  $SiO_2$ - $K_2O$ - $CaO$  glass degradation due to atmospheric dry depositions. *Atmos. Environ.* **2012**, *55*, 459–466. [[CrossRef](#)]
6. Palomar, T.; Oujja, M.; García-Heras, M.; Villegas, M.A.; Castillejo, M. Laser induced breakdown spectroscopy for analysis and characterization of degradation pathologies of Roman glasses. *Spectrochim. Acta Part B At. Spectrosc.* **2013**, *87*, 114–120. [[CrossRef](#)]
7. Melcher, M.; Wiesinger, R.; Schreiner, M. Degradation of glass artifacts: Application of modern surface analytical techniques. *Acc. Chem. Res.* **2010**, *43*, 916–926. [[CrossRef](#)]
8. Palomar Sanz, T. Effect of soil pH on the degradation of silicate glasses. *Int. J. Appl. Glass Sci.* **2017**, *8*, 177–187. [[CrossRef](#)]
9. Jackson, C.M.; Greenfield, D.; Howie, L.A. An assessment of compositional and morphological changes in model archaeological glasses in an acid burial matrix. *Archaeometry* **2012**, *54*, 489–507. [[CrossRef](#)]
10. Licenziati, F.; Falcone, R.; Orsega, E.F. Marco Verità Studio preliminare sulla produzione e il degrado di vetri potassici e sodici come modelli di vetrate artistiche e di vetri industriali in ambiente confinato. *Riv. Stn. Sper. Vetro* **2010**, *3*, 7–17.

11. Terreni, L.G. Le problematiche conservative del vetro antico proveniente da scavi archeologici. *Riv. Millarium* **2007**, *8*, 34–47.
12. Silvestri, A.; Molin, G.; Salviulo, G. Roman and medieval glass from the Italian area: Bulk characterisation and relationships with production technologies. *Archaeometry* **2005**, *47*, 797–816. [[CrossRef](#)]
13. Verità, M. Analisi di reperti vitrei e scarti di lavorazione di tarda età romana provenienti dagli scavi del monastero di Santa Giulia a Brescia. In *Santa Giulia di Brescia: Gli scavi dal 1980 al 1992*; Brogiolo, G.P., Morandini, F., Rossi, F., Eds.; Reperti Preromani, Romani e Altomedievali All’Insegna dell’Giglio, Publisher: Firenze, Italia, 1999; pp. 309–314.
14. Werner, V. *Glass Chemistry*, 2nd ed.; Springer: Berlin/Heidelberg, Germany, 1994.
15. Scholze, H. *Glass Nature, Structure and Properties*; Springer: New York, NY, USA, 1991.
16. Verità, M. *Modern and Ancient Glass: Nature, Composition and Deterioration Mechanisms, the Materials of Cultural Heritage in Their Environment, Centro Universitario per i Beni Culturali, Ravello*; EdiPuglia: Bari, Italy, 2006.
17. Davison, S.; Newton, R. *Conservation and Restoration of Glass*, 2nd ed.; Butterworth-Heinemann: Oxford, UK, 2007.
18. Das, C.R.; Douglas, R.W. Studies on the reaction between water and glass. Part 3. *Phys. Chem.* **1967**, *8*, 178–184.
19. Varshneya, K. *Fundamentals of Inorganic Glass*; Academic Press: New York, NY, USA, 1993.
20. Walters, H.V.; Adams, P.B. Effects of Humidity on the weathering of glass. *J. Non-Cryst. Solids* **1975**, *19*, 183–199. [[CrossRef](#)]
21. Munier, I.; Lefèvre, R.A.; Losno, R. Atmospheric factors influencing the formation of Neocrystallisation on low durability glass expose to urban atmosphere. *Glass Technol.* **2002**, *43*, 114–124.
22. Geotti-Bianchini, F.; Preo, M. *Fattori Rilevanti per Prevenire Alterazione Idrolitica (“Ossidazione”) del Vetro Float*; Rivista della Stazione Sperimentale del Vetro.: Rome, Italy, 1999; Volume 3, pp. 127–140.
23. Bianchini-Geotti, F.; Nicola, C.; Preo, M.; Vallotto, M.; Verità, M. *MicroIRRS and EPMA Study of the Weathering of Potash-Lime-Silicate Glasses*; Rivista della Stazione Sperimentale del Vetro.: Rome, Italy, 2005; Volume 3, pp. 49–61.
24. Munier, I.; Lefèvre, R.A.; Geotti-Bianchini, F.; Verità, M. Influence of polluted urban atmosphere on the weathering of low durability glasses. *Glass Technol-Part A* **2002**, *43*, 225–237.
25. Falcone, R.; Nardone, M.; Sodo, A.; Sommariva, G.; Vallotto, M.; Verità, M. SEM-EDS, EPMA and MRS analysis of neo-crystallisations on weathered glasses. *Mater. Sci. Eng.* **2010**, *7*, 1–7. [[CrossRef](#)]
26. Lombardo, T.; Chabas, A.; Lefevre, R.A.; Verità, M.; Geotti-Bianchini, F. Weathering of a float glass exposed outdoor in urban area. *Glass Technol.* **2005**, *46*, 271–276.
27. Verità, M.; Falcone, R.; Sommariva, G.; Chopinet, M.H.; Lehuédé, P. Weathering of the inners surface of soda-lime-silica glass containers exposed to the atmosphere. *Glass Technol-Part A* **2009**, *50*, 65–70.
28. Fermo, P.; Andreoli, M.; Bonizzoni, L.; Fantauzzi, M.; Giubertoni, G.; Ludwig, N.; Rossi, A. Characterisation of Roman and Byzantine glasses from the surroundings of Thugga (Tunisia): Raw materials and colour. *Microchem. J.* **2016**, *129*, 5–15. [[CrossRef](#)]
29. Andreoli, M. Glass finds from a Late Antique-Byzantine farm at Ain Ouassel (Tunisia). *Antiq. Afr.* **2015**, *51*, 219–233. [[CrossRef](#)]
30. Andreoli, M. Reperti vitrei. In *Rus Africum IV. La Fattoria Bizantina di Ain Wassel, Africa Proconsularis (Alto Tell, Tunisia)*; Raaijmakers deVos, M., Maurina, B., Eds.; Archaeopress: Oxford, UK, 2019; pp. 302–312.
31. Cappelletti, G.; Ardizzone, S.; Fermo, P.; Gilardoni, S. The influence of iron content on the promotion of the zircon structure and the optical properties of pink coral pigments. *J. Eur. Ceram.* **2005**, *25*, 911–917. [[CrossRef](#)]
32. Gunther, D.; Heinrich, C.A. Enhanced sensitivity in laser ablation-ICP mass spectrometry using helium-argon mixtures as aerosol carrier. *J. Anal. At. Spectrom.* **1999**, *14*, 1363–1368. [[CrossRef](#)]
33. Barca, D.M.; Abate, G.M.; Crisci, D.; Presbiteris, D. Post-Medieval glass from the castle of Cosenza, Italy: Chemical characterization by LA-ICP-MS and SEM-EDS. *Per. Min.* **2009**, *78*, 49–64.
34. Barca, D.; Basso, E.; Bersani, D.; Galli, G.; Invernizzi, C.; La Russa, M.F.; Lottici, P.P.; Malagodi, M.; Ruffolo, S.A. Vitreous tesserae from the calidarium mosaics of the Villa dei Quintili, Rome. Chemical composition and production technology. *Microchem. J.* **2016**, *124*, 726–735. [[CrossRef](#)]
35. Barca, D.; Papparella, F.C. Chemical, characterization of vitreous finds from Cosenza cathedral (Calabria-Italy) by the combined use of analytical techniques. *Archaeology* **2020**, *6*, 63–85.

36. Fiorenza, E.; Rovella, N.; D'andrea, M.; Musella, M.; Sudano, F.; Taliano Grasso, A.; Barca, D. Vitreous tesserae from the Four Seasons Mosaic of S. Aloe quarter in Vibo Valentia–Calabria, Italy: A chemical characterization. *Minerals* **2020**, *10*, 658. [CrossRef]
37. Schreiner, M.; Melcher, M.; Uhlir, K. Scanning electron microscopy and energy dispersive analysis: Applications in the field of cultural heritage. *Anal. Bioanal. Chem.* **2007**, *387*, 737–747. [CrossRef]
38. Bonizzoni, L.; Bruni, S.; Guglielmi, V.; Milazzo, M.; Neri, O. Field and laboratory multi-technique analysis of pigments and organic painting media from an Egyptian coffin (26th dynasty). *Archaeometry* **2011**, *53*, 1212–1230. [CrossRef]
39. Bruni, S.; Guglielmi, V.; Della Foglia, E.; Castoldi, M.; Bagnasco, G. A non-destructive spectroscopic study of the decoration of archaeological pottery: From matt-painted bichrome ceramic sherds (southern Italy, VIII-VII B.C.) to an intact Etruscan cinerary urn. *Spectrochim. Acta A* **2018**, *191*, 88–97. [CrossRef]
40. Palomar Sanz, T.; García Heras, M.; Sáiz-Jiménez, C.; Márquez Goncer, C.; Villegas Broncano, M.Á. Technical Note: Pathologies and analytical study of mosaic materials from Carmona and Italica. *Mater. Constr.* **2011**, *61*, 629–636. [CrossRef]
41. Abd-Allah, R. Chemical cleaning of soiled deposits and encrustations on archaeological glass: A diagnostic and practical study. *J. Cult. Herit.* **2013**, *14*, 97–108. [CrossRef]
42. Palomar, T.; Garcia Herasa, M.; Sabiob, R.; Rinconc, J.M.; Villegasa, M.A. Composition, preservation and production technology of Augusta Emerita roman glasses from the first to the sixth century AD. *Mediterr. Archaeol. Archaeom.* **2012**, *12*, 193–211.
43. Fantauzzi, M.; Pacella, A.; Atzei, D.; Gianfagna, A.; Andreozzi, G.B.; Rossi, A. Combined use of X-ray photoelectron and Mössbauer spectroscopic techniques in the analytical characterization of iron oxidation state in amphibole asbestos. *Anal. Bioanal. Chem.* **2010**, *396*, 2889–2898. [CrossRef]
44. De Vos, M. *Terra Acqua e Olio Nell'africa Settentrionale. Scavo e Ricognizione nei Dintorni di DOUGGA (Alto Tell Tunisino)*; Africum, R., Ed.; Temi: Trento, Italia, 2000.
45. Raaijmakers deVos, M.; Maurina, B. *La Fattoria Bizantina di Ain Wassel, Africa Proconsularis (Alto Tell, Tunisia)*; Africum, R., IV, Ed.; Archaeopress: Oxford, UK, 2019.
46. Dal Bianco, B.; Bertoncetto, R. The development of growth rings on ancient glass surfaces: Description and simulation of the weathering. *J. Non. Cryst. Solids* **2008**, *354*, 773–779. [CrossRef]
47. Newton, R.G. The durability of glass, a review. *Glass Technol.* **1984**, *26*, 21–38.
48. Tournié, A.; Ricciardi, P.; Colomban, P.H. Glass corrosion mechanisms: A multiscale analysis. *Solid State Ionics* **2008**, *179*, 2142–2154. [CrossRef]
49. Barbana, F.; Bertoncetto, R.; Milanese, L.; Sada, C. Alteration and corrosion phenomena in Roman submerged glass fragments. *J. Non. Cryst. Solids* **2004**, *337*, 136–141. [CrossRef]
50. Retrieve Data for a Selected Element. Available online: <https://srdata.nist.gov/xps/selEnergyType.aspx> (accessed on 21 September 2020).

**Publisher's Note:** MDPI stays neutral with regard to jurisdictional claims in published maps and institutional affiliations.



© 2020 by the authors. Licensee MDPI, Basel, Switzerland. This article is an open access article distributed under the terms and conditions of the Creative Commons Attribution (CC BY) license (<http://creativecommons.org/licenses/by/4.0/>).